https://doi.org/10.31436/iiumej.v26i3.3603

FORMATION OF VOID IN BFS/$CACO_3$ DIFFUSION COUPLE

AHMAD ABDUL MUN'IM ISMAIL[1*], ALYA NAILI ROZHAN[1], MUHAMMAD RAFIQ HAIKAL ROSDIN[1], HADI PURWANTO[2], ABD MALEK ABDUL HAMID[1], M. H. ANI[1]

[1] Department of Manufacturing and Materials, Kulliyyah of Engineering, International Islamic University Malaysia, Jalan Gombak, 53100 Kuala Lumpur, Malaysia.
[2] Department of Engineering Management, Universitas Internasional Semen Indonesia, Kompleks PT. Semen Indonesia (Persero) Tbk. Jl. Veteran, Gresik Jawa Timur, 61122 Indonesia.

**Corresponding author: imismalz@gmail.com*

(Received: 31 January 2025; Accepted: 28 May 2025; Published online: 9 September 2025)

ABSTRACT: This study investigates void formation in the blast furnace slag (BFS) and calcium carbonate ($CaCO_3$) diffusion couple, which is critical for understanding the interdiffusion process in cement production. The experimental analysis involved high-temperature diffusion experiments, focusing on the volume fraction of void at the BFS/$CaCO_3$ interface, the activation energy of void formation, and the I-V measurement of void formation at the BFS/$CaCO_3$ interface. Void measurements revealed a 25% increase after exposure to the specified temperature, while the activation energy for void formation was calculated to be – 41.48 kJ/mol. I-V measurements revealed ionic diffusion as the dominant mechanism for void formation, with an average decomposition rate of 1.4598×10^{-12} m^2s^{-1}. These findings provide valuable insights for utilizing BFS in cement production.

ABSTRAK: Kajian ini menyelidik pembentukan rongga dalam pembentukan sanga relau letupan (BFS) dan kalsium karbonat ($CaCO_3$), di mana ianya sangat penting bagi memahami proses antara resapan (interdiffusion) dalam pengeluaran simen. Analisis eksperimen melibatkan ujian resapan pada suhu tinggi, dengan tumpuan kepada pecahan isipadu rongga antara permukaan BFS/$CaCO_3$, tenaga pengaktifan bagi pembentukan rongga, dan pengukuran I-V bagi pembentukan rongga antara muka BFS/$CaCO_3$. Pengukuran rongga menunjukkan peningkatan sebanyak 25% selepas terdedah kepada suhu yang ditetapkan, manakala tenaga pengaktifan bagi pembentukan rongga dikira sebanyak –41.48 kJ/mol. Pengukuran I-V menunjukkan bahawa penyebaran ionik merupakan mekanisme dominan bagi pembentukan rongga, dengan kadar penguraian purata sebanyak 1.4598×10^{-12} m^2/s. Dapatan ini memberikan pemahaman penting bagi penggunaan BFS dalam pengeluaran simen.

KEYWORDS: *void formation, diffusion couple, blast furnace slag, calcium carbonate*

1. INTRODUCTION

The study of void formation in the BFS/$CaCO_3$ diffusion couple explores the mechanisms underlying solid-state diffusion and the implications of this process on material properties. Blast Furnace Slag (BFS), a byproduct of the iron and steel industry, contains valuable chemical components, including calcium oxide (CaO) and silicon dioxide (SiO_2). Its utilization in cement production, particularly when combined with calcium carbonate ($CaCO_3$), presents an opportunity to reduce waste and improve resource efficiency[1], [2], [3]. However, understanding the diffusion behavior [4], [5] between these materials, particularly the

https://doi.org/10.31436/iiumej.v26i3.3603

formation of voids, is crucial to optimizing the production process and ensuring the structural integrity of the final product.

Solid-state diffusion, which occurs in materials with lattice imperfections, plays a pivotal role in the chemical reactions between BFS and $CaCO_3$ [6], [7]. The diffusion of calcium ions (Ca^{2+}) from $CaCO_3$ into BFS leads to the formation of calcium silicate phases such as alite (Ca_3SiO_5) and belite (Ca_2SiO_4)[8], [9]. These phases are critical in cement production as they contribute to the strength and durability of the material. However, the formation of voids during this diffusion process can compromise the material's mechanical properties, necessitating a thorough investigation into the factors influencing void formation[10], [11].

Previous studies have shown that the diffusion of ions such as Ca^{2+} is influenced by temperature, concentration gradients, and the presence of impurities [12], [13], [14]. The introduction of foreign elements, such as aluminum oxide (Al_2O_3) or iron oxide (Fe_2O_3), can further complicate the diffusion process by altering the reaction kinetics and contributing to void formation[15], [16]To better understand these phenomena, this research examines the diffusion behavior of BFS and CaCO3 under various temperature conditions, focusing on the relationship between ion migration and void formation.

Void formation during solid-state diffusion is a complex process influenced by the interaction of multiple variables. During these reactions, voids are frequently observed at the interface due to the solid-state diffusion of Ca^{2+} ions from $CaCO_3$ into BFS. Therefore, this study focused on the volume fraction of voids, their activation energy, and the role of alite and belite phases for understanding the BFS-$CaCO_3$ cement and the efficiency of the clinker formation process.

2. METHODOLOGY

2.1. Furnace Design and Setup

A high-temperature vertical furnace was employed for the diffusion experiments. The furnace's temperature was monitored using a Type R thermocouple, capable of measuring temperatures up to 1723 K, which was positioned at the center of the furnace to ensure accurate readings. An alumina tube, measuring 1000 mm long with an outer diameter of 60 mm and an inner diameter of 50 mm, served as the reaction chamber. The BFS and $CaCO_3$ samples were horizontally clamped together using wire gauze and placed within the furnace's isothermal zone, which was determined to be 100 mm long.

2.2. Sample Preparation

BFS and $CaCO_3$ were ground into fine powders using an alumina mortar and pestle to achieve homogeneity. The powders were then pressed into cylindrical pellets, each 10 mm in diameter and approximately 3 mm thick. These pellets were sintered in an air environment at 873 K for six hours. One side of each pellet was mechanically polished using P2000 grit emery paper to ensure optimal contact during the diffusion experiments. The polished BFS and $CaCO_3$ samples were then paired and clamped together with wire gauze to form the diffusion couple, as shown in Fig. 1. BFS and $CaCO_3$ samples were prepared and subjected to high-temperature conditions (1273 K, 1323 K, and 1373 K) for varying time periods (86.4 ks, 259 ks, and 432 ks).

https://doi.org/10.31436/iiumej.v26i3.3603

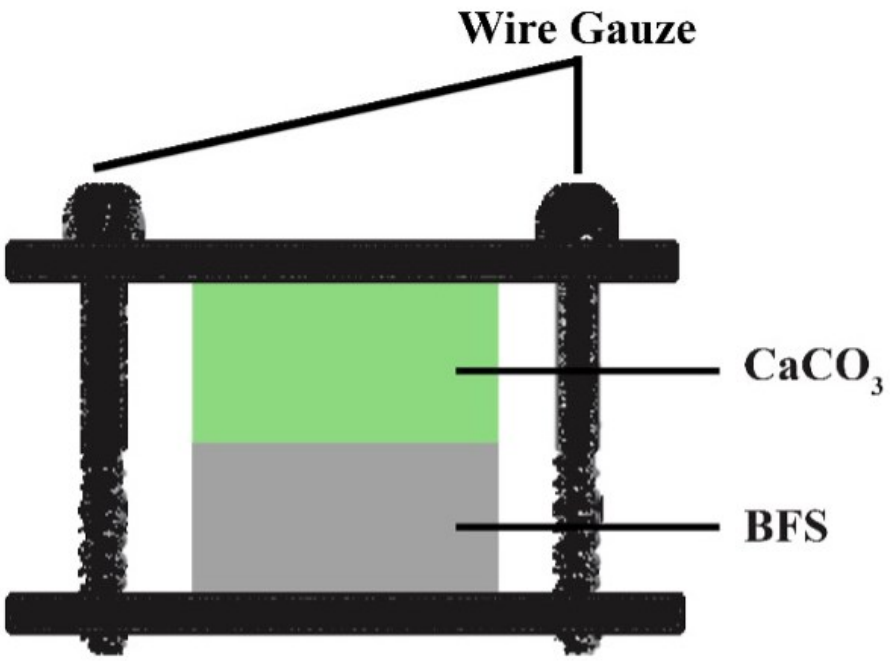

Figure 1. Schematic illustration of BFS/CaCO3 diffusion couple.

2.3. Characterization and Evaluation

The elemental composition of the BFS/$CaCO_3$ diffusion couple was analyzed before and after the diffusion process using X-ray Diffraction (XRD) and Scanning Electron Microscopy with Energy Dispersive X-ray analysis (SEM-EDX). XRD analysis, performed with a Bruker D2 Phaser using Cu Kα radiation, confirmed the composition of the samples before diffusion. Post-diffusion, SEM-EDX analysis (JEOL JSM-IT100) was conducted at 10 kV to investigate the elemental distribution across the sample's cross-section. The samples were prepared for SEM-EDX by mounting them in resin and sectioning with a diamond cutter to expose the cross-section.

2.4. Void Formation Calculation and Analysis

The diffusion coefficient of calcium ions (Ca^{2+}) from $CaCO_3$ into BFS was calculated using the Boltzmann-Matano method, which involves analyzing the concentration profile of the diffusing species. The concentration profiles were obtained from the SEM-EDX analysis and used to determine the diffusivity of Ca^{2+} ions. Additionally, the volume fraction of voids formed during the diffusion process was calculated using the formula proposed by [17] and [18] Where v_{void}^{ox} represents the formation of voids within the scale during the oxidation process, l pertains to the inner scale, and L corresponds to the outer scale with L > 1. $(L - l)^3$ is used to convert the void formation into cubic dimensions, mirroring the actual structure of the oxide scale diffused into the sample.

$$f_v = \frac{v_{void}^{ox}}{(L-l)^3} \quad (1)$$

2.5. Diffusion Couple I-V Experiment

The diffusion experiments involved setting up a tracer diffusion couple, where platinum wire electrodes were used for both working and counter electrodes due to their high melting point and chemical resistance. The experiment was conducted at 1373 K, and the potential difference between the electrodes was measured over time. Tafel plots were generated to

https://doi.org/10.31436/iiumej.v26i3.3603

evaluate the electrochemical reaction rate, which provided insights into the diffusion of ions, particularly Ca2+, within the BFS/CaCO3 system. The reaction rate was calculated using the Tafel slope, which quantitatively measures ion transport in the diffusion couple. [19], [20], [21]

This methodology outlines a comprehensive approach to studying the formation of voids in the BFS/CaCO3 diffusion couple. It uses SEM, EDX, XRD, and I-V experiments to provide detailed insights into the formation of voids impacted by diffusion behaviors.

3. RESULTS AND DISCUSSION

3.1. Volume Fraction of Voids In the BFS/$CaCO_3$ Interface

SEM images showed significant void formation at the BFS/$CaCO_3$ interface after prolonged exposure at high temperatures. Voids were observed as annealing time and temperature increased. The formation of voids in limestone, as depicted in Fig. 2, occurs due to the release of CO_2 gas into the atmosphere when exposed to high temperatures. In these conditions, CO_2 becomes volatile and escapes from the limestone. Several studies have explored the mechanism behind void formation in limestone. For instance, when limestone is heated, a chemical reaction occurs, releasing CO_2 gas as a byproduct [22]. The trapped gas creates internal pressure, and if this pressure cannot escape, voids or bubbles form within the material [23]. Additionally, higher temperatures accelerate the decomposition reaction, causing a more rapid release of CO_2 gas, which leads to pressure gradients that contribute to void formation [24]. In the case of BFS-limestone, void formation is driven by the Kirkendall effect, where uneven diffusion rates between species cause voids at the interface [25].

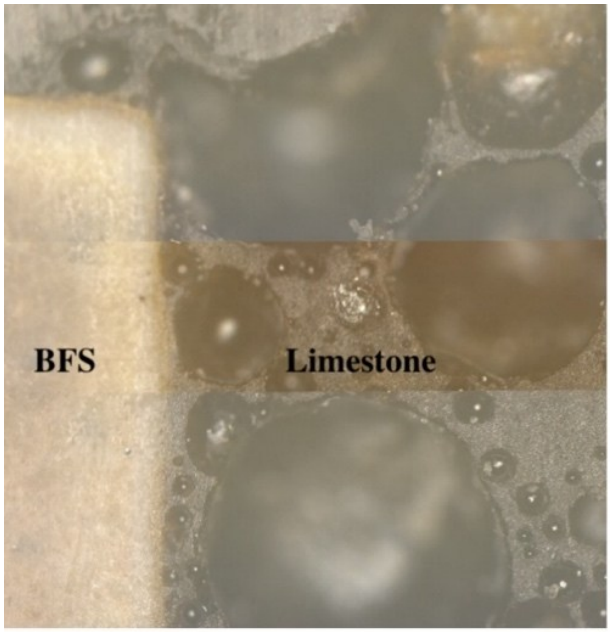

Figure 2. Formation of void in Limestone from one of the cross sections exposed to 1373 K at 432ks.

Fig. 3 shows the distribution of voids across the limestone, interlayer oxide, and BFS regions. The SEM image highlights a higher concentration of voids in the limestone area, with fewer voids observed in the interlayer oxide and BFS regions. To confirm this observation, the void percentage in each region can be calculated using the formula provided in Equation 1.

https://doi.org/10.31436/iiumej.v26i3.3603

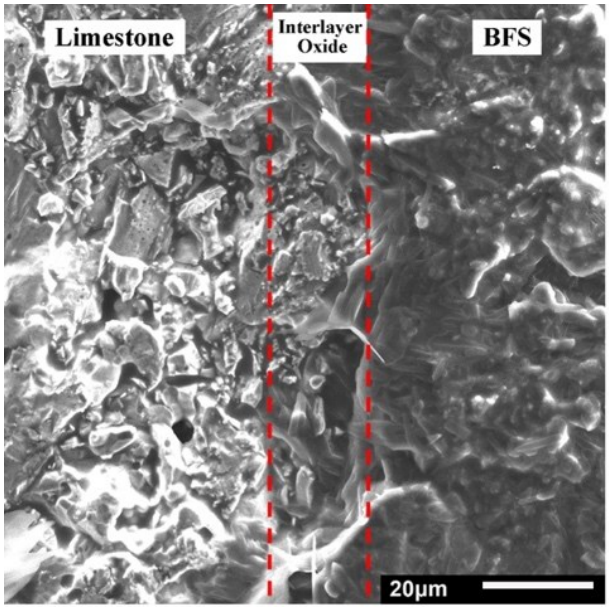

Figure 3. Cross-sectional micrograph of BFS/CaCO3 diffusion couple from one of the cross sections exposed to 1373 K at 432ks. The red dashed line indicates the interlayer oxide boundary.

Fig. 4 demonstrates that the volume fraction of voids decreases with longer exposure times, plateauing by 432 ks. This suggests that the $CaCO_3$ has fully reacted, CO_2 has been completely released, and no further voids are formed. In the early stages, the $CaCO_3$ actively releases CO_2, resulting in a higher void concentration at the BFS/$CaCO_3$ interface. Samples exposed to lower temperatures, such as 1273 K, exhibit fewer voids than those exposed to 1323 K and 1373 K. At the initial exposure time, the difference in void volume fraction reaches up to 30%. However, the void fractions for samples at 1323 K and 1373 K are pretty similar, as these temperatures approach the vaporization point of $CaCO_3$. The data show that the volume fraction of voids aligns well with the governing equation 1.

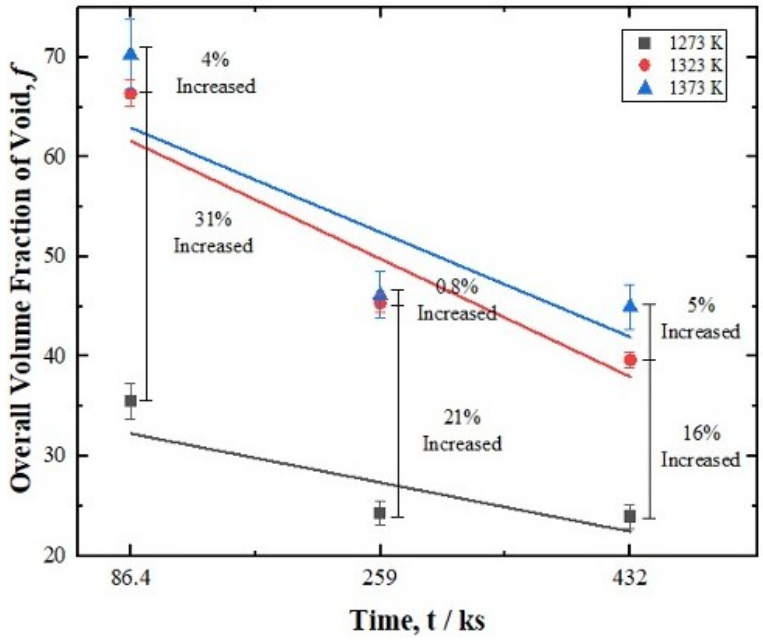

Figure 4. Overall Volume Fraction of Void vs Time

https://doi.org/10.31436/iiumej.v26i3.3603

Figure 4 also illustrates that higher temperatures increase void volume, ranging from 0.8% to 31%. As exposure time increases, void formation decreases and stabilizes. Overall, the void formation drops by 14%. The figure also suggests that increasing temperature will cause the void fraction to reach a steady state, implying that the void percentage may remain constant with prolonged exposure at higher temperatures.

Further analysis of the void percentage in the BFS, interlayer oxide, and limestone regions, as shown in Figures 5 (a), (b), and (c), reveals a clear distinction in void formation. Figure 5 (a) shows that the reaction is still unstable; therefore, the voids at the three-phase boundary do not exhibit a clear pattern. As the temperature increases, the limestone region shows the highest volume of voids, followed by the BFS and the interlayer oxide, as seen in Figures 5 (b) and 5 (c). This is attributed to the decomposition of limestone, where the release of CO_2 at elevated temperatures generates more voids in the limestone region.

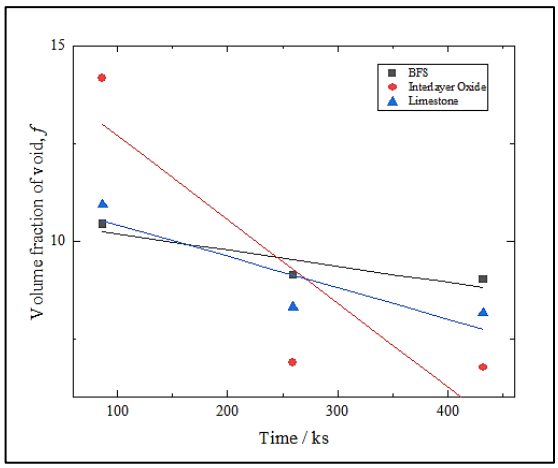

(a) Void at 1273K

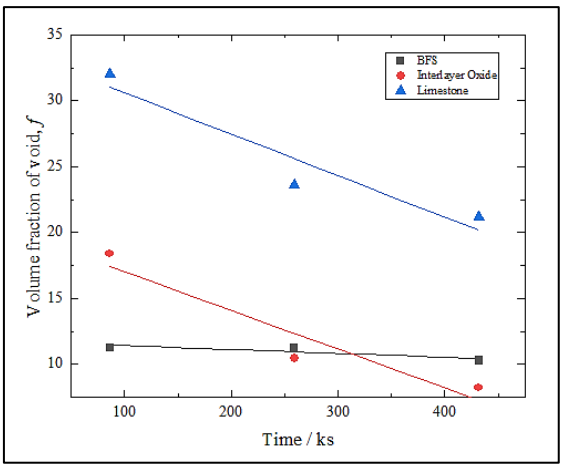

(b) Void at 1323K

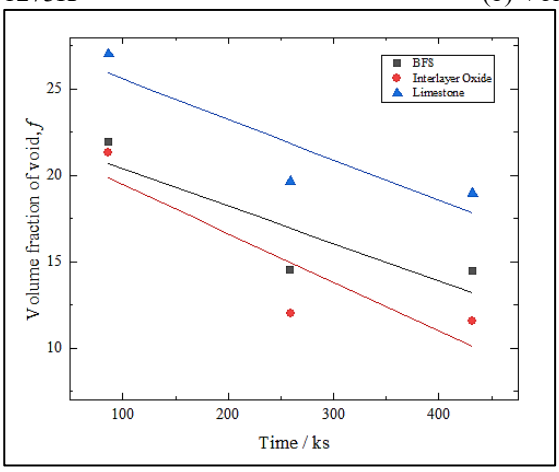

(c) Void at 1373K

Figure 5. Volume Fraction of Void at each layer vs Time at (a) 1273 K (b) 1323 K and (c) 1373 K

3.2 Activation Energy of Void Formation

Figure 6 illustrates the temperature dependence of the overall volume fraction of voids, showing a proportional increase that aligns with the trend in Figure 5. The void fraction is directly related to the rate of CO_2 volatilization and can be described using the Arrhenius equation. The void fraction, f, can be expressed using the Arrhenius equation as shown in Equation (2), where f_o is the pre-exponential function and Q is the void activation energy. The

https://doi.org/10.31436/iiumej.v26i3.3603

figure shows a linear relationship between log f and 1/T, representing the first reaction order. The activation energy for void formation, Q, was determined as – kJ/mol.

$$log\, f = log\, f_o - \frac{Q}{RT} \quad (2)$$

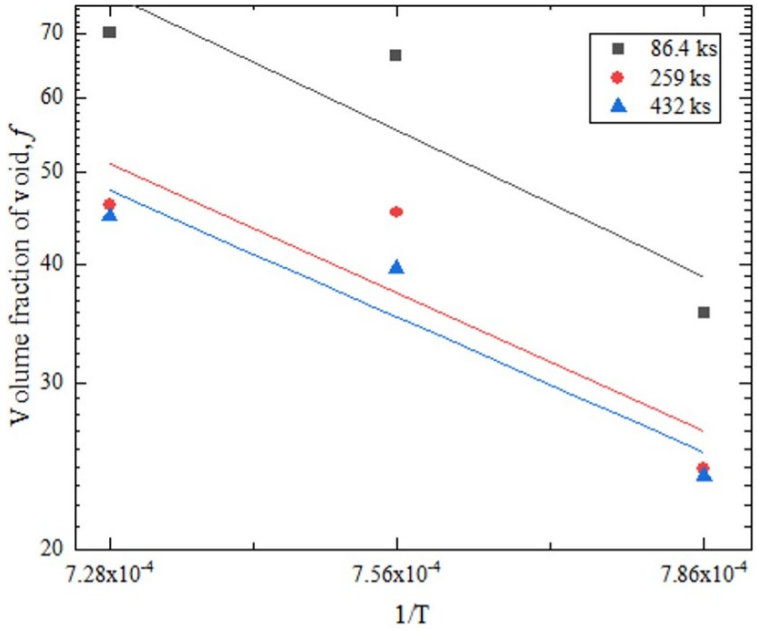

Figure 6. Overall Volume Fraction of Void vs Temperature

By plotting the logarithm of void volume fraction against inverse temperature, the activation energy for void formation was calculated. Table 1 shows the activation energy of void formation at the respective conditions. The longer the BFS/CaCO3 is exposed to the respective temperature, the energy for void formation at the respective couples is reduced. It shows the activation energy reduced by 7% at 432 ks.

Table 1. The activation energy for void formation, Q.

Reaction Time/ks	Activation Energy / kJ·mol^{-1}
86.4	−43.43
259	−40.90
432	−40.10

Further analysis can be done on the void fraction of BFS, interlayer oxide, and limestone, which can be referred to in Figures 7 (a), (b), and (c). A clear distinction can be observed based on this figure, where the highest volume of voids formed is in limestone, followed by BFS and interlayer oxide accordingly. This phenomenon confirms the reaction equation $CaCO_3(s) \rightarrow CaO\ (s) + CO_2\ (g)$, where CO_2 is gasified at high temperature. Thus, the volume fraction of void in the limestone area is the highest.

https://doi.org/10.31436/iiumej.v26i3.3603

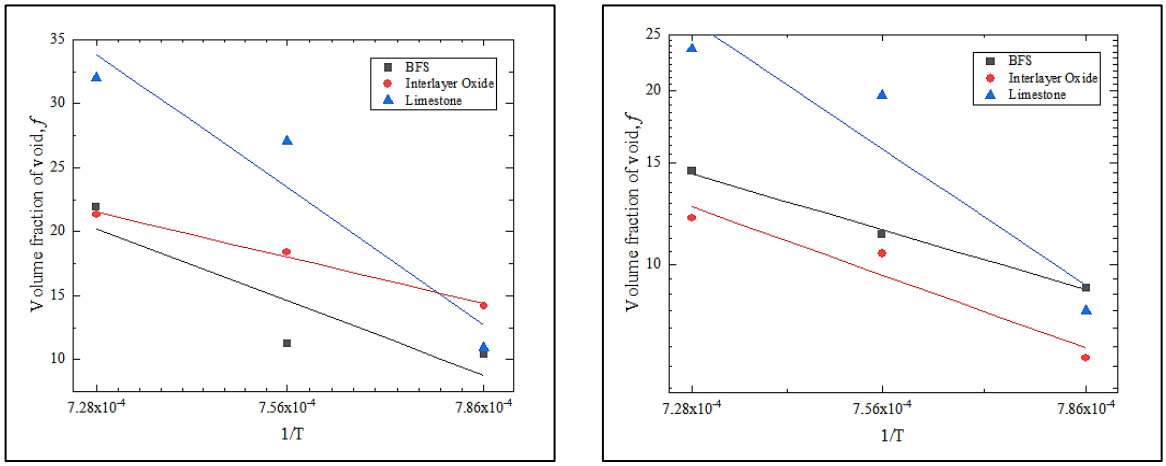

(a) Void at 86.4 ks (b) Void at 259 ks

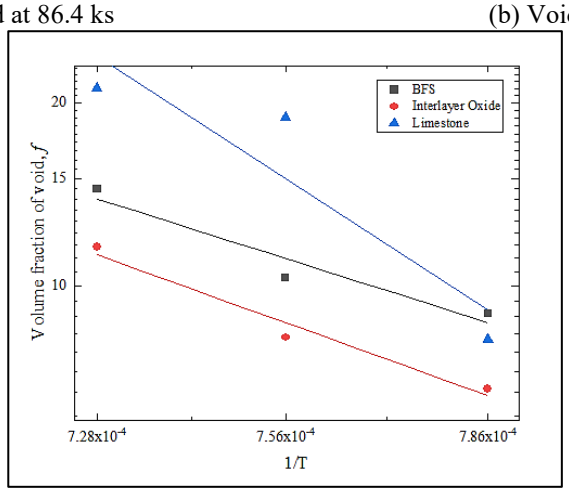

(c) Void at 432 ks

Figure 7. Volume Fraction of Void at each layer vs 1/T at (a) 86.4 ks (b) 259 ks and (c) 432 ks

3.3. I-V Measurement of Void Formation at BFS/$CaCO_3$ Interface

The I-V measurements were performed using platinum electrodes. The Tafel plot analysis revealed a linear relationship between the applied voltage and the current density, indicating that ionic diffusion is the dominant mechanism in void formation. The Tafel slope was used to calculate the reaction rate, which increased with temperature, confirming the temperature dependence of the diffusion process. Figure 8 presents the I-V plot of the BFS/$CaCO_3$ diffusion couple exposed to 1373 K for 60 s, 180 s, 300 s, 420 s, and 540 s. The I-V curve can be used to determine $E_{reaction}$ and $I_{reaction}$, which correspond to the potential and current from the main reaction in the diffusion couple. All results follow the Tafel pattern, allowing for the calculation of $E_{reaction}$ by finding the intersection points where a tangent line meets both the anodic and cathodic curves.

A notable observation is the rightward shift of the Tafel plot at 420 s compared to 300 s. This shift is due to the ongoing reaction between BFS and limestone, forming a diffusion oxide layer. As the reaction progresses, more calcium and oxygen are consumed, increasing the diffusion layer's formation. The rightward shift indicates that equilibrium has not yet been reached. Once the reaction involving the oxide layer is complete, the system undergoes another transition, as calcium and oxygen from the BFS/CaCO3 components continue to react. This leads to the leftward shift observed in the 540s Tafel plot, signifying that the calcium-oxygen reaction has become dominant and the system has reached a more stable state.

https://doi.org/10.31436/iiumej.v26i3.3603

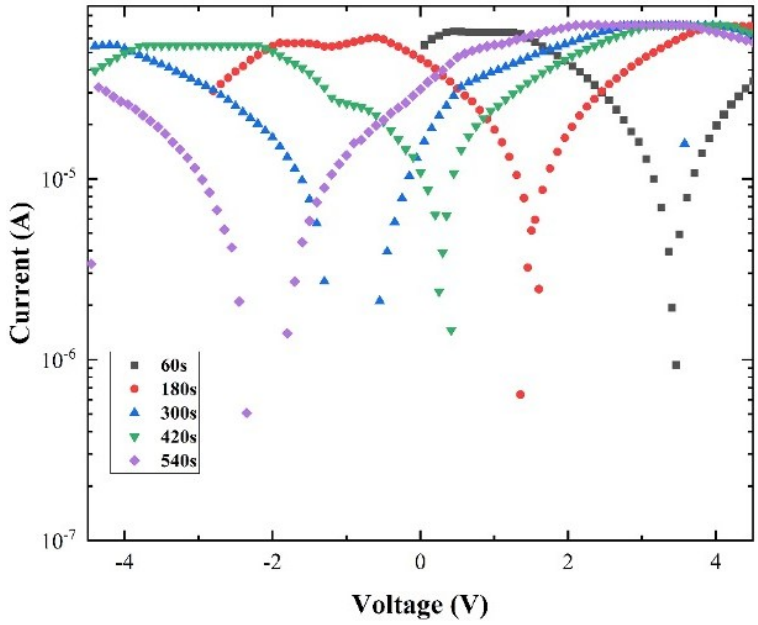

Figure 8. Tafel Plot of BFS/CaCO3 diffusion couple exposed to 1373 K at various time frames.

The $E_{reaction}$ from Figure 8 reflects the value from the decomposition of CaCO3. Over time, the decomposition rate is expected to decrease due to the reduced surface area, causing the curve to shift to the left. This leftward shift in the Tafel plot indicates a change in the dominant reaction within the diffusion couple, showing the system is reaching a more stable state. Additionally, the I-V plot can be used to calculate the Tafel slope and reaction rate, which are summarized in the decomposition rates in Table 2.

Table 2. Corresponding values calculated from the Tafel plot.

Time / s	$E_{reaction}$ / V	$I_{reaction}$ / A	Reaction rate (10^{-12}) / m^2s^{-1}
60	3.58	1.56 x 10^{-5}	1.6735
180	1.5	1.49 x 10^{-5}	1.5984
300	- 0.977	1.64 x 10^{-5}	1.7593
420	0.141	1.49 x 10^{-5}	1.5984
540	- 2.125	6.24 x 10^{-6}	0.6694

4. CONCLUSION

This study highlights the significance of void formation at the BFS/CaCO3 interface during high-temperature diffusion processes, which plays a crucial role in the interdiffusion process for cement production. The findings indicate a 25% increase in void volume after exposure to specific temperatures, with the activation energy for void formation calculated at –41.48 kJ/mol. Ionic diffusion was identified as the dominant mechanism for void formation, with an average decomposition rate of 1.4598 × 10^{-12} m^2s^{-1}. These insights are valuable for optimizing the use of BFS in cement production.

ACKNOWLEDGEMENT

This research was financially supported by the Ministry of Higher Education, Malaysia, with Grant Number FRGS/1/2019/TK07/UIAM/03/3.

REFERENCES

[1] T. Gao, L. Shen, M. Shen, L. Liu, and F. Chen, "Analysis of material flow and consumption in cement production process," *J Clean Prod*, vol. 112, pp. 553–565, Jan. 2016, doi: 10.1016/j.jclepro.2015.08.054.

[2] A. A. M. Ismail, M. R. H. Rosdin, A. M. A. Hamid, H. Purwanto, A. N. Rozhan, and M. H. Ani, "Producing Blast Furnace Slag Cement Clinker by Utilizing Redox Reaction Approach," 2023, pp. 89–96. doi: 10.1007/978-981-19-1851-3_8.

[3] A. A. M. Ismail *et al.*, "Blast Furnace Slag Cement Clinker Production Using Limestone-Hot Blast Furnace Slag Mixture," 2023, pp. 539–545. doi: 10.1007/978-981-19-9509-5_71.

[4] T. Tian, Y. Zhang, H. Zhang, K. Zhang, J. Li, and H. Wang, "Dissolution behavior of SiO2 in the molten blast furnace slags," *Int J Appl Ceram Technol*, vol. 16, no. 3, pp. 1078–1087, May 2019, doi: 10.1111/ijac.13120.

[5] M. Matsushima, S. Yadoomaru, K. Mori, and Y. Kawai, "Fundamental Study on the Dissolution Rate of CaO into Liquid Slag," *Tetsu-to-Hagane*, vol. 62, no. 2, pp. 182–190, 1976, doi: 10.2355/tetsutohagane1955.62.2_182.

[6] J. Zheng, X. Hu, Z. Ren, X. Xue, and K. Chou, "Solid-state reaction studies in Al2O3-TiO2 system by diffusion couple method," *ISIJ International*, vol. 57, no. 10, pp. 1762–1766, 2017, doi: 10.2355/isijinternational.ISIJINT-2017-042.

[7] S. Yasipourtehrani, S. Tian, V. Strezov, T. Kan, and T. Evans, "Development of robust CaO-based sorbents from blast furnace slag for calcium looping CO2 capture," *Chemical Engineering Journal*, vol. 387, p. 124140, May 2020, doi: 10.1016/j.cej.2020.124140.

[8] Y. A. Mohamed, A. E. M. O. Kasif, E. A. A. Alla, and M. M. Elmahadi, "Calculation of the formation process of clinker inside the rotary cement kiln," *Proceedings of the Voronezh State University of Engineering Technologies*, vol. 80, no. 1, pp. 233–239, Apr. 2018, doi: 10.20914/2310-1202-2018-1-233-239.

[9] S. Telschow, "Clinker Burning Kinetics and Mechanism," 2012.

[10] M. Li, S. Chen, H. Dai, H. Zhao, and B. Jiang, "Experimental Investigation on the Mass Diffusion Behaviors of Calcium Oxide and Carbon in the Solid-State Synthesis of Calcium Carbide by Microwave Heating," *Molecules*, vol. 26, no. 9, p. 2568, Apr. 2021, doi: 10.3390/molecules26092568.

[11] X. Zhang, W. J. Meng, and A. C. Meng, "Chemical potential gradient induced formation of Kirkendall voids at the epitaxial TiN/MgO interface," *Nanoscale*, vol. 15, no. 31, pp. 13086–13093, 2023, doi: 10.1039/D3NR01860A.

[12] A. Shankar, M. Görnerup, A. K. Lahiri, and S. Seetharaman, "Experimental Investigation of the Viscosities in CaO-SiO2-MgO-Al2O3 and CaO-SiO2-MgO-Al2O3-TiO2 Slags," *Metallurgical and Materials Transactions B*, vol. 38, no. 6, pp. 911–915, Dec. 2007, doi: 10.1007/s11663-007-9087-5.

[13] M. Chen, W. Zhang, Z. Zhao, T. Evans, and B. Zhao, "Effects of Minor Elements to the Liquidus Temperatures of Blast Furnace Slags," *ISIJ International*, vol. 56, no. 12, pp. 2156–2160, 2016, doi: 10.2355/isijinternational.ISIJINT-2016-268.

[14] Z. S. Ren, X. H. Hu, and K. C. Chou, "Model for diffusion coefficient estimation of calcium ions in CaO–Al $_2$ O $_3$ –SiO $_2$ slags," *Ironmaking & Steelmaking*, vol. 40, no. 8, pp. 625–629, Nov. 2013, doi: 10.1179/1743281212Y.0000000090.

[15] Y. Wang, X. Liu, H. Wang, and K. Vecchio, "The effect of oxides on Fe/Al interfacial reaction in Metal-Intermetallic Laminate (MIL) composites," *J Alloys Compd*, vol. 845, p. 156268, Dec. 2020, doi: 10.1016/j.jallcom.2020.156268.

[16] O. A. Bulavchenko *et al.*, "The Influence of Cu and Al Additives on Reduction of Iron(III) Oxide: *In Situ* XRD and XANES Study," *Inorg Chem*, vol. 58, no. 8, pp. 4842–4850, Apr. 2019, doi: 10.1021/acs.inorgchem.8b03403.

[17] M. Ueda, K. Kawamura, and T. Maruyama, "Void Formation in Magnetite Scale Formed on Iron at 823 K -Elucidation by Chemical Potential Distribution-," *Materials Science Forum*, vol. 522–523, pp. 37–44, Aug. 2006, doi: 10.4028/www.scientific.net/MSF.522-523.37.

[18] A. Kaderi, A. Z. Mohd Zainal, M. H. Ani, and R. Othman, "Observation On Void Formed In Oxide Scale Of Fe-Cr-Ni Alloy At 1073k In Dry And Humid Environments," *IIUM Engineering Journal*, vol. 12, no. 5, Jan. 2012, doi: 10.31436/iiumej.v12i5.235.

[19] M. E. G. Lyons and M. P. Brandon, "Redox switching and oxygen evolution electrocatalysis in polymeric iron oxyhydroxide films," *Physical Chemistry Chemical Physics*, vol. 11, no. 13, p. 2203, 2009, doi: 10.1039/b815338h.

[20] P. Bai and M. Z. Bazant, "Charge transfer kinetics at the solid–solid interface in porous electrodes," *Nat Commun*, vol. 5, no. 1, p. 3585, Apr. 2014, doi: 10.1038/ncomms4585.

[21] N. M. Marković, B. N. Grgur, and P. N. Ross, "Temperature-Dependent Hydrogen Electrochemistry on Platinum Low-Index Single-Crystal Surfaces in Acid Solutions," *J Phys Chem B*, vol. 101, no. 27, pp. 5405–5413, Jul. 1997, doi: 10.1021/jp970930d.

[22] T. T. Belete, M. C. M. Van De Sanden, and M. A. Gleeson, "Effects of transition metal dopants on the Calcination of CaCO3 under Ar, H2O and H2," *Journal of CO2 Utilization*, vol. 31, pp. 152–166, May 2019, doi: 10.1016/j.jcou.2019.03.006.

[23] F. Van Loock, V. Bernardo, M. A. Rodríguez Pérez, and N. A. Fleck, "The mechanics of solid-state nanofoaming," *Proceedings of the Royal Society A: Mathematical, Physical and Engineering Sciences*, vol. 475, no. 2230, 2019, doi: 10.1098/rspa.2019.0339.

[24] M. Benitez-Guerrero, B. Sarrion, A. Perejon, P. E. Sanchez-Jimenez, L. A. Perez-Maqueda, and J. Manuel Valverde, "Large-scale high-temperature Solar Energy storage using Natural Minerals," *Solar Energy Materials and Solar Cells*, vol. 168, pp. 14–21, Aug. 2017, doi: 10.1016/j.solmat.2017.04.013.

[25] [Y. F. Gong and B. C. De Cooman, "Kirkendall void formation during selective oxidation," *Metall Mater Trans A Phys Metall Mater Sci*, vol. 41, no. 9, pp. 2180–2183, Sep. 2010, doi: 10.1007/s11661-010-0356-6.